Magalhães, P. R., Oliveira, A. S. F., Campos, S. R. R., Soares, C. M., & Baptista, A. M. (2017). Effect of a pH Gradient on the Protonation States of Cytochrome c Oxidase: A Continuum Electrostatics Study. *Journal of Chemical Information and Modeling*, *57*(2), 256-266. https://doi.org/10.1021/acs.jcim.6b00575

Effect of a pH Gradient on the Protonation States of Cytochrome *c* Oxidase: A Continuum Electrostatics Study

Pedro R. Magalhães, A. Sofia F. Oliveira, Sara R. R. Campos, Cláudio M. Soares, and António M. Baptista*

Instituto de Tecnologia Química e Biológica António Xavier, Universidade Nova de Lisboa, 2781-901 Oeiras, Portugal

E-mail: baptista@itqb.unl.pt

Phone: +351 214469619

Abstract

Cytochrome *c* oxidase (C*c*O) couples the reduction of dioxygen to water with transmembrane proton pumping, which leads to the generation of an electrochemical gradient. In this study we analyze how one of the components of the electrochemical gradient, the difference in pH across the membrane, or ΔpH , influences the protonation states of residues in C*c*O. We modified our continuum electrostatics/Monte Carlo (CE/MC) method in order to include the ΔpH and applied it to the study of C*c*O, in what is, to our best knowledge, the first CE/MC study of C*c*O in the presence of a pH gradient. The inclusion of a transmembrane pH gradient allows for the identification of residues whose titration behavior depends on the pH on both sides of the membrane. Among the several residues with unusual titration profiles, three are well known key residues in the proton transfer process of C*c*O: $E286_I$, $Y288_I$ and $K362_I$. All three residues have been previously identified as being critical for the catalytic or proton

pumping functions of C*c*O. Our results suggest that when the pH gradient increases, these residues may be part of a regulatory mechanism to stem the proton flow.

Introduction

Cytochrome *c* oxidase (C*c*O) is an integral membrane protein complex that catalyzes the final step in the electron transport chain of mitochondria and some species of aerobic bacteria.[1] This enzyme is a member of the heme-copper oxidase superfamily, which is divided into three main families: A, B and C, according to the differences in the pathways and mechanisms of proton transfer. Family A oxidases, also known as mitochondrial-like oxidases, can be further subdivided into two groups: type A1 and type A2, depending on a conserved sequence of residues at the end of one of the proton conducting channels.[2] In this work, we will focus on type A1 oxidases, which include some of the most widely studied systems, such as the bovine heart mitochondria, *Paracoccus denitrificans* and *Rhodobacter sphaeroides* enzymes.[3] Type A1 oxidases share structural similarities in their core functional unit, composed of subunits I and II (Figure 1A).[2] Subunit I, which is also known as the catalytic subunit, contains a low-spin heme (heme *a*) and a high-spin heme (heme a_3). Heme a_3, together with a copper ion (Cu_B) form the so-called binuclear center. Subunit II contains a binuclear copper center (Cu_A) which receives the electrons from cytochrome *c*.[2]

Cytochrome *c* oxidase couples the reduction of O_2 to H_2O with the transfer of protons across the membrane. It was determined experimentally that in the bovine heart mitochondria, *P. denitrificans* and *R. sphaeroides* oxidases, this reaction follows a stoichiometry of one proton pumped per electron, as shown in Eq. 1.[3]

$$4\ \mathrm{cytc}_\mathrm{P}^{2+} + 8\ \mathrm{H}_\mathrm{N}^{+} + \mathrm{O}_2 \leftrightarrows 2\ \mathrm{H}_2\mathrm{O} + 4\ \mathrm{cytc}_\mathrm{P}^{3+} + 4\ \mathrm{H}_\mathrm{P}^{+} \tag{1}$$

The protons required for the reduction of O_2 come from the negative (N), or inner, side of the membrane (H_N^+), whereas the electrons from the oxidation of cytochrome *c* ($cytc_P^{2+}$)

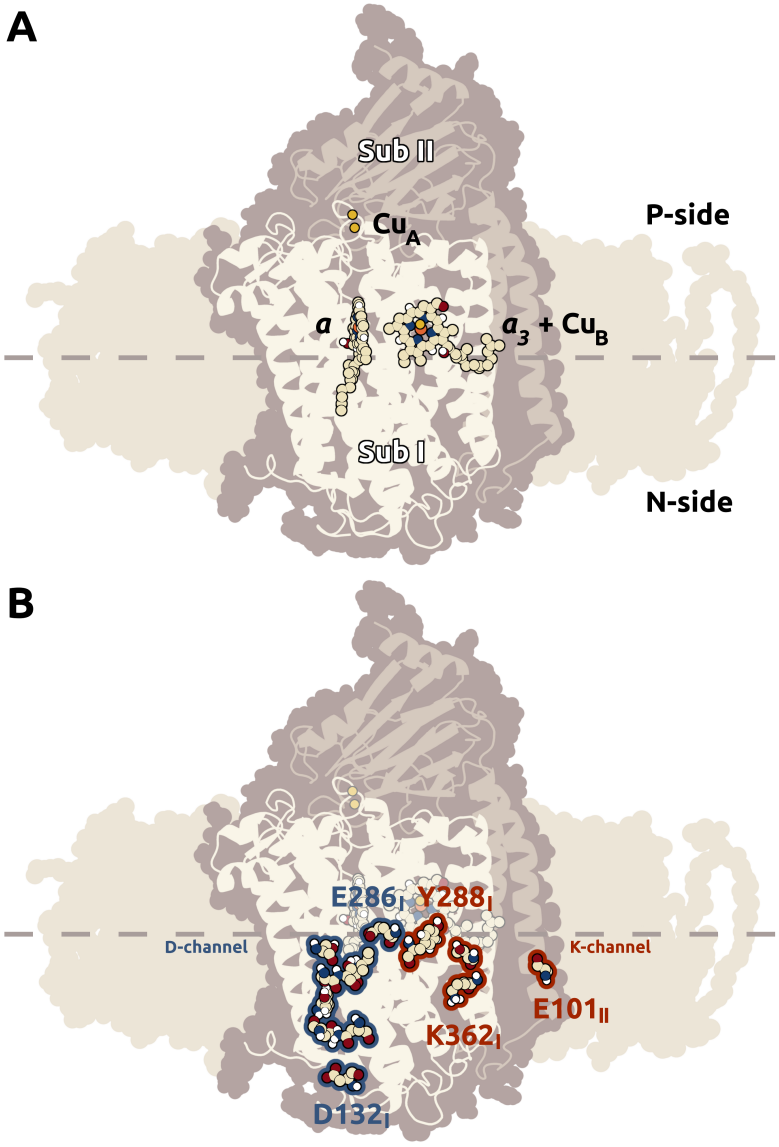

Figure 1: Schematic representation of the subunits and redox centers in C*c*O (A) and the residues that comprise the D and K proton conducting channels (B). The crystallographic water molecules in both channels are hidden for clarity. All figures showing depictions of molecules were made using the PyMOL graphics package[4] and the GNU Image Manipulation program.[5]

come from the positive (P), or outer, side. Of the eight protons involved in this reaction, only four are required for the reduction of O_2. The remaining four protons are pumped across the membrane, from the N- to the P-side (H_P^+), which contributes to generation of a transmembrane electrochemical gradient. Both chemical and pumped protons are transported by two input channels: the D-channel and the K-channel (Figure 1B).[6]

The largest of the two proton conducting channels, the D-channel, contains a highly conserved aspartic acid residue, $D132_I$ (*R. sphaeroides* numbering is used throughout this paper), which is located at the surface of the N-side of the protein, and gives the channel its name. The channel contains a network of water molecules leading to an important glutamic acid residue, $E286_I$, which is located approximately within 10 Å of the binuclear center in subunit I. The D-channel transports between two and three of the four chemical protons required for the reduction of dioxygen, as well as all four pumped protons.[7]

The K-channel transports the remaining one or two chemical protons required for catalysis, and its entry point is thought to be located near $E101_{II}$.[8,9] The protons are then transported to $K362_I$, a highly conserved lysine residue after which the channel is named. The channel ends at another conserved residue near the active site of the oxidase: $Y288_I$.[10]

A third channel, named after a conserved histidine residue ($H456_I$),[11] has also been identified: the H-channel. Although $H456_I$ and some of the other hydrophilic residues that are part of the H-channel are conserved in oxidases from different species, some key residues are absent in bacteria, resulting in an incomplete network when compared to the mitochondrial oxidase, for instance. Point mutations were performed on several residues of this channel which resulted in a decrease of enzymatic activity in mitochondrial oxidases, but not in bacterial oxidases.[12,13] Although these studies showed that the H-channel is only relevant as a proton conducting pathway in mitochondrial C*c*O, an alternative role for this channel in bacteria was proposed as a dielectric channel, which is a channel with a high dielectric strength that connects the protein surface and a buried center, and that, despite its inability to conduct a proton current, provides a pathway of dielectric relaxation

for the transient introduction of a charge into the center.[14–16]

The role of the residues lining the D- and K-channels has been studied both experimentally and computationally (reviewed in Refs. 7 and 17, respectively) using different techniques, but some details of the proton transfer mechanism are still not fully understood, particularly when taking into account the effect of the generated electrochemical gradient. The electrochemical gradient has an electrical and a chemical component: respectively, the membrane potential ($\Delta\psi$), and the difference in pH across the membrane (ΔpH).[18] Although it is possible to perform experimental studies of proton pumps in the presence of these gradients (e.g. Refs. 19, 20 21 and 22), their inclusion in computational approaches is usually not performed. Ullmann and co-workers[23] included a pH gradient in their continuum electrostatics/Monte Carlo (CE/MC) study of bacteriorhodopsin, which allowed them to determine how this gradient affected the titration of key residues involved in proton transfer. In a later study, they also included a transmembrane potential in the computational study of bacteriorhodopsin, and it was shown to also affect the protonation state of key residues.[24] Although it has been suggested that the pH gradient is not as significant as the membrane potential as a component of the electrochemical gradient in some of these systems,[18] these two studies by Ullmann and co-workers have shown that the ΔpH can significantly affect the titration of several residues, meaning that its presence is an important factor to consider when studying this type of protein.

In this work, we modified our current CE/MC method[25,26] in order to include a pH gradient and applied this new implementation to the study of cytochrome *c* oxidase. Our results show that the titration of several residues is affected by the pH gradient across the membrane, particularly the titration of key residues known to be involved in the proton transfer process of C*c*O.

Methods

System setup

We used the fully oxidized state of C*c*O from *R. sphaeroides* (PDB ID: 2GSM[27]) as the starting structure. All metal centers and non-standard residues were parameterized as described in a recent publication.[28] Only the core functional unit, composed by subunits I and II, is included in this X-ray structure. An explicit bilayer with 256 1-2-dimyristoyl-*sn*-glycero-3-phosphocholine (DMPC) molecules was added to the starting structure using the GROMACS genbox tool.[29,30] Lipid molecules clashing with the protein were automatically removed, resulting in a bilayer with 172 DMPC molecules. SPC water[31] molecules were added, and the system's energy was minimized for 5000 steps using the steepest descent algorithm,[32] followed by 10^4 steps using the limited-memory Broyden-Fletcher-Goldfarb-Shanno algorithm.[32] The system was then initialized for 20 ns with all protein atoms heavily restrained in order to allow the lipid molecules to adapt to the protein structure. Lastly, in order to completely remove any residual motion of groups during the initialization process, the resulting protein structure was replaced by the starting x-ray structure. The relative accessibility of x-ray water molecules to the solvent was performed using ASC,[33,34] and all non-crystallographic water molecules and those with a relative accessibility above 50% were removed after this process. The resulting structure was used in the continuum electrostatics calculations.

Energy minimization and initialization simulations were performed using GROMACS 4.0.7[29,30] and the GROMOS 54A7 force field.[35] Periodic boundary conditions were used in a tetragonal unit cell. Non-bonded interactions were treated using a twin-range method[36] with short- and long-range cutoffs of 8 Å and 14 Å, respectively, and with the neighbor lists updated every 5 steps. In addition, the long-range electrostatics interactions were treated using the generalized-reaction-field method.[37] Bond lengths were constrained using the LINCS algorithm[38] and an integration time step of 1 fs was used due to the high restraints

imposed on the protein structure, as previously mentioned. Temperature coupling was performed using the v-rescale thermostat,[39] and the temperature was set to 310 K using a coupling constant of 0.05 ps. A semi-isotropic pressure coupling was performed using the Berendsen barostat.[40] The compressibility was set to 4.6×10^{-5} bar^{-1} and the coupling constant was set to 10 ps.

CE/MC calculations

Finite difference Poisson-Boltzmann calculations were performed using MEAD 2.2.9.[41] A three-step focusing procedure was used for the protein and membrane system, with the first grid composed of 161^3 points, each spaced 2.0 Å, the second grid composed of 81^3 points, each spaced 1.0 Å and with the third grid composed of 81^3 points each spaced 0.25 Å. A two-step focusing procedure was used for the model compounds using 61^3 grid points spaced 1.0 Å and 0.25 Å for the first and second grids, respectively. Protein and lipid atoms were assigned partial charges and radii derived from the GROMOS 54A7 force field[35] as previously described.[42] Proton isomerism was included as tautomeres for the neutral forms of all titratable sites and as rotamers for water molecules and serine and threonine residues, as described elsewhere.[26,28,42] The pK values of the model compounds were the ones previously used by Oliveira et al.[43] The molecular surface was defined with a solvent probe radius of 1.4 Å, and a Stern ion-exclusion layer of 2.0 Å. A temperature of 300 K and an ionic strength of 0.1 M were used. Dielectric constants of 80 and 10 were assigned respectively to the solvent and to the protein/membrane regions. When applied at the molecular level, the dielectric constant of non-solvent regions is essentially an empirical parameter that attempts to capture all factors not explicitly included in the model used,[44,45] such as structural reorganization, being highly dependent on the nature of this model.[45] Thus, different CE/MC methodologies must be compared as a whole, since their parameters are tightly related (e.g., a higher inner dielectric constant may be needed to compensate for the radii of united atoms and the generally higher dipoles occurring in

GROMOS force fields). Our CE/MC method typically needs a moderately large dielectric constant in the absence of full structural sampling, requiring a value of 6 or 8 even when limited reorganization is explicitly included.[44,46] Thus, since the CE/MC calculations are performed in the present work using a single rigid structure, a dielectric constant of 10 was chosen. Furthermore, a value of 10 was found to accurately reproduce the protonated state of the retinal in the ground state of bacteriorhodopsin, used for testing the present methodology "Method validation" below).

Monte Carlo (MC) calculations were performed using the newest version of our in-house program PETIT[25,26] which was modified in order to include a pH gradient. Unlike the previous implementations of PETIT, where all titratable sites are exposed to a single pH value, this newer version requires the pre-assignment of sites to two different proton baths named 'N' and 'P' (after the two sides of the membrane), each with a particular pH value. The first step of the method is this assignment of sites to either the N- or the P-side. This was performed by selecting all lipid molecules within a 30 Å radius of the center of the protein, and using the average z coordinates of the phosphorous atoms of each monolayer to calculate a membrane midpoint. Using a simple geometric criterion, the z coordinates of the functional groups of titratable residues were then compared to the membrane midpoint, and assigned to either the N- or the P-side if they were below or above it, respectively. The only site which had to be manually assigned due to its location near the midpoint was $E286_I$. Given that the side chain of this residue is facing down towards the N-side in all x-ray structures,[47] we decided to assign it to this side. The assignment results in a two-column file identifying all titratable residues and their corresponding assignment to one of the proton baths. This file is then used by PETIT, along with two user-specified parameters: the pH and the ΔpH. The program will use the ΔpH value in order to calculate the values of pH_N and pH_P using: $pH_{input} \pm (\Delta pH/2)$. The sampling of protonation states is then performed as in previous implementations,[26,42] but using the modification discussed in detail by Ullmann and co-workers:[23] instead of using a

single pH value when computing the global free energy change due to the capture/release of protons, each individual site-specific term uses the pH value of its assigned membrane side, i.e., pH_N or pH_P (see eq. 4 in reference 23).

Calculations were performed for all combinations of pH values in the 0–14 range using an interval of 0.1 pH units, and in the 5–9 range using an interval of 0.025 units. Each MC run consisted of 10^3 equilibration steps followed by 10^5 production steps (or 10^6 steps for the calculation of correlation values), with one step corresponding to a cycle of single trial protonation moves on each site plus a cycle of double trial moves on each pair of strongly-coupled sites (with an interaction above 2 pK_a units). Trial moves were evaluated with a Metropolis scheme[48] using the Poisson-Boltzmann protonation energy terms and the pH of the solution, as previously described.[23,26]

Method validation

The implementation of pH gradients in our continuum electrostatics method was tested using a simpler system, namely bacteriorhodopsin, and by comparing the results with those that Ullmann and co-workers obtained using their in-house software, which also included a pH gradient.[23] Bacteriorhodopsin is perhaps the most well studied proton pumping system. It is an archaeal light-driven proton pump, composed of seven transmembrane helices and with a retinal chromophore, which, when stimulated by light, triggers a series of conformational events that lead to a proton being transferred from the N- to the P-side of the membrane.[49] The starting structure of bacteriorhodopsin was prepared following the protocol of Ullmann and co-workers, using the high-resolution ground state structure (PDB ID: 1C3W[50]) as the main structure, and building the missing loops with Modeller 9v6[51–54] using an x-ray structure of bacteriorhodopsin grown in lipidic cubic phases obtained at 1.9 Å (PDB ID: 1QHJ[55]). In addition, both termini were capped. The atomic partial charges for the retinal group were parameterized using quantum chemical methods. Protons were energy optimized using Gaussian09[56] by keeping the positions of the heteroatoms fixed.

Optimizations were performed using B3LYP/6-31G(d). Single-point calculations were then performed on the resulting optimized structures using B3LYP and cc-pVTZ basis sets. Solvent effects were included using PCM in a medium with a dielectric constant value of 4. The RESP method[57] was then used for the derivation of atomic partial charges for the atoms of interest, which can be found in the supporting information (Figure S1). Bonds and van der Waals parameters were adapted from the GROMOS 54A7 force field, whereas angles and dihedrals around the nitrogen atom were parameterized using a quantum/molecular mechanical approach.[58] The construction of the membrane system and initialization protocol were performed as described for C*c*O, using the same parameters. Poisson-Boltzmann calculations were then performed at 293 K, using an ionic strength value of 1 M and a dielectric constant value of 10. The assignment of titratable sites to a side of the membrane was performed as described for C*c*O, which resulted in all sites being assigned in agreement with the method used by Ullmann and co-workers.[23] MC calculations were then performed for all combinations of pH values in the 0–16 range, every 0.1 pH units, using 10^3 equilibration steps and 10^4 MC steps.

Ullmann and co-workers[23] reported that six out of the total 39 titratable residues in bacteriorhodopsin exhibited an irregular titration behavior that was dependent on the pH values on both sides of the membrane. Our method was able to correctly identify the same six irregularly titrating residues: D85, D96, D115, E194, E204, and the retinal group (Figure S2 in the supporting information). Overall, in the terms of the dependence on the pH gradient, our results are in agreement with those of Ref. 23, e.g. our method was able to correctly model the antagonistic behavior described by Ullmann and co-workers between the two titration curves of D85 and the retinal group which is in agreement with the fact that a proton is transferred between the two residues. In addition, calculations were also performed in which D115, a residue which is located in the very center of the protein and that was manually assigned to either the N- or the P-side in calculations performed by Ullmann and co-workers, was also assigned to either the N- or the P-sides of the membrane

in different calculations. This assignment was found to have some effect, although small, on the titration of the other key residues, also in agreement with Ullmann and co-workers, as observed in Figure S2 in the supporting information. Although the same trends were observed, it is worth noting some differences in the titration curves between our results and those of Ref. 23, which can be attributed to two main factors: the different charges and radii, whose underlying force field is united-atom in the present work, and all-atom in the work by Ullmann and co-workers; the different non-solvent dielectric constants, which in the present work is higher than the one used in Ref. 23. (Preliminary tests showed that the use of different membrane models, explicit in the present work and implicit in Ref. 23, does not significantly affect the results.) In any case, as already noted above, molecular CE models are largely empirical, meaning that these two types of parameters are closely related and that different methodologies should be compared as a whole. This view is reinforced by the fact that, despite their different methodologies, the same overall trend was found in both works for all titratable residues, particularly for those found to be influenced by the pH gradient.

Results and discussion

Types of titration behavior

The titration profiles of some residues in C*c*O,[59] as well as in other proton pumps,[23,60] may deviate from the standard Henderson–Hasselbalch sigmoid behavior due to strong electrostatic interactions with other residues. In addition to this, the titration curves become even more complex by the inclusion of different pH values on both sides of the membrane. In order to depict how the the titration profiles of residues were affected by the pH on the N- and P-sides of the membrane, two-dimensional titration curves were plotted for all residues of C*c*O (Figure S3 in the supporting information). As observed for bacteriorhodopsin,[23] three different types of titration behavior were identified (Figure 2):

(i) residues that did not titrate at any pH value, namely buried residues that are closely interacting with other nearby residues or water molecules (e.g. $Y146_I$ and $E539_I$); (ii) residues whose titration is only affected by the pH of the side they were assigned to, which are usually exposed residues that titrate without being influenced by the pH on the other side of the membrane (e.g. $E86_I$ and $R137_I$); and lastly, (iii) residues whose titration is affected by the pH gradient (e.g. $Y422_I$ and $H456_I$), which are the ones this work will focus on.

Although there are several residues which exhibit a titration curve that is influenced by the pH gradient, most of them only titrate at extreme pH values, as exemplified by residues $Y422_I$ and $H456_I$ (Figure 2). Despite this, it is worth noting that one of these residues, $H456_I$, is a conserved histidine in the H-channel. Given that it has been shown by mutation experiments that the H-channel in bacteria is not critical for the function of C*c*O,[62] the biological relevance of this dependence on the pH gradient is not clear.

Identification of key residues

Among the several residues whose titration is influenced by the pH gradient, three are particularly noteworthy, mostly because this effect can be observed at physiological pH values (Figure 3). These residues are: Glutamate 286 ($E286_I$), Tyrosine 288 ($Y288_I$) and Lysine 362 ($K362_I$). As mentioned in the introduction section, $E286_I$, $Y288_I$ and $K362_I$ are key residues in C*c*O and are all part of the proton conduction channels of the protein ($E286_I$ of the D-channel; $Y288_I$ and $K362_I$ of the K-channel) and as expected, all three of these residues play critical roles in the proton transfer mechanism of C*c*O.

$E286_I$ is located at the very end of the D-channel, near the active site of C*c*O. It has been suggested that this residue, due to its proximity to the catalytic site, serves as a regulator of the flow of chemical and pumped protons, both of which are transported through the D-channel. The side chain of $E286_I$ has been observed to be in contact with the N-side of the membrane when facing down towards the D-channel as in our study, and indeed as in

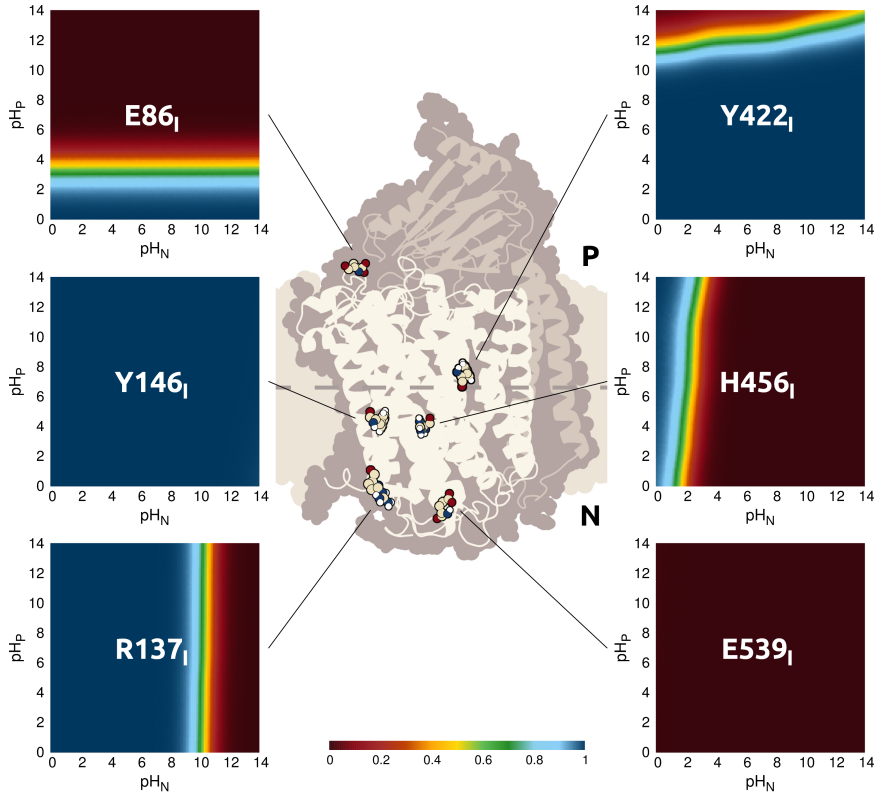

Figure 2: Two-dimensional titration curves of some residues in C*c*O. The protonation is shown in a color scale from red (deprotonated, 0) to blue (protonated, 1). The location of the residues in the protein is also shown in the center figure. All plots were made using Gnuplot 4.4.[61]

all x-ray structures of C*c*O.[27,63,64] An upward facing conformation of this side chain has also been proposed through an interaction with the D-propionate of heme a_3 as part of a valve mechanism[47,65,66] which would prevent the leakage of protons to the N-side of the membrane back through the D-channel in the direction of the gradient.

$Y288_I$ is a highly conserved residue among heme-copper oxidases and is the terminal residue in the K-channel,[2] located within hydrogen-bonding distance of the hydroxyl group of the farnesyl side chain of heme a_3. This tyrosine is a very particular residue: it is covalently bound to one of the histidine residues that coordinates Cu_B ($H284_I$), by a post-translational modification.[63,64] It has been postulated that $Y288_I$ is directly involved in the catalytic process of C*c*O, by donating a hydrogen atom to facilitate the breaking of the O–O bond.[11]

$K362_I$ is another highly conserved residue. It is located in a hydrophobic environment, approximately 15 Å below the binuclear center.[14] It is located near the entrance of the K-channel, and appears to provide a direct pathway for substrate protons to reach the hydroxyl moiety of $Y288_I$ at the active site of the enzyme, despite the absence of a fully connected water network.[11,67] It is also worth noting that in the available crystal structures[27,63,64] the side chain of $K362_I$ points downward in the direction of the N-side of the protein, instead of up and bridging the gap between the entrance and the binuclear center, as would perhaps be expected, given the distance between the side chain of $K362_I$ and the other residues in the K-channel near the active site (e.g. $Y288_I$). Molecular dynamics simulations have shown that the side chain of $K362_I$ is flexible enough to accomplish this motion.[28,68,69]

pK_a values in the absence of a pH gradient

As we can observe in Figure 3B, in the absence of a gradient, the titration curves for $E286_I$, $Y288_I$ and $K362_I$ retain a sigmoidal appearance. The midpoint pK_a values calculated for all three residues are very similar: $pK_a(E286_I) = 7.9$, $pK_a(Y288_I) = 7.4$, $pK_a(K362_I) = 7.6$.

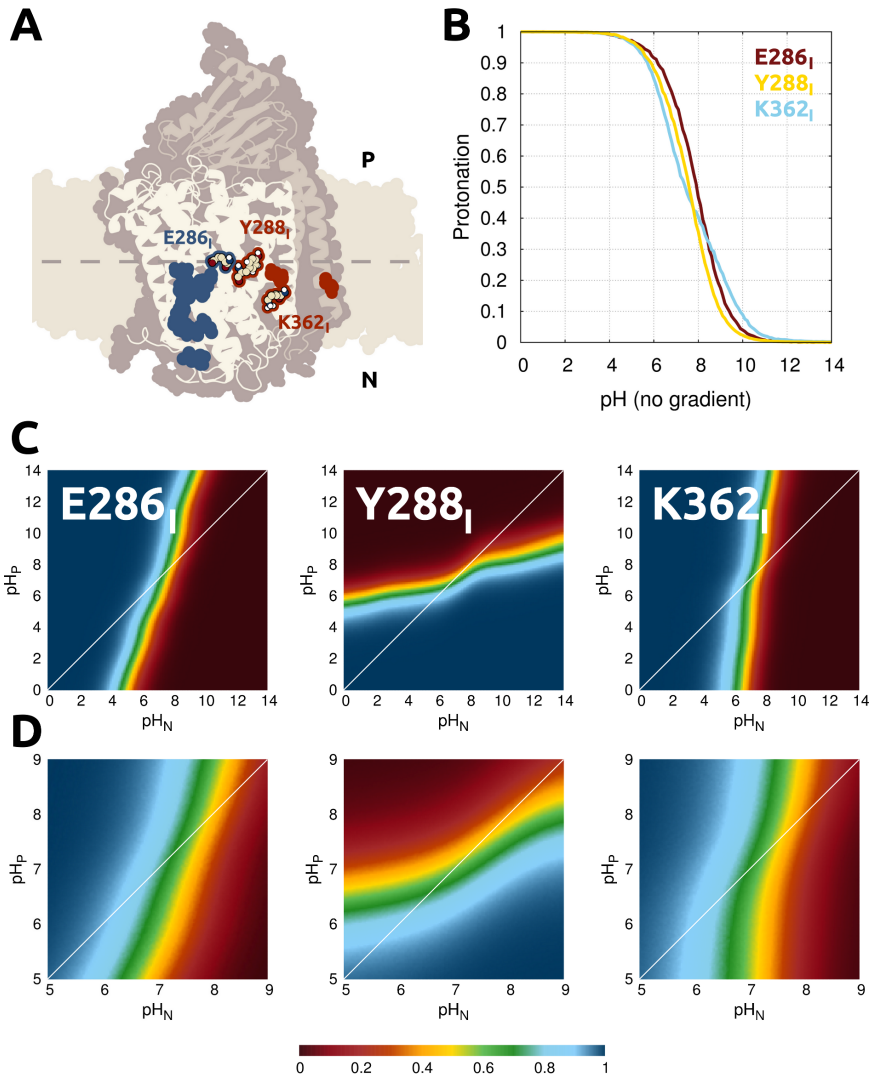

Figure 3: Location of $E286_I$, $Y288_I$ and $K362_I$ in C*c*O (A). The blue outline shows the other residues in the D-channel, and the red outline shows the other residues in the K-channel. Also shown are the titration curves for the three residues without any gradient present (B) and in the presence of a pH gradient (C). In addition, the close-ups of the white squared region in C are also shown (D). The diagonal white lines represent the case where no pH gradient is present (i.e. the curves shown in B).

The pK_a values of all residues are shown in table S1 in the Supporting Information.

Regarding $E286_I$, it has been reported that this particular glutamic acid residue has an unusually high pK_a value when compared to solution, which is in agreement with the value of 7.9 we obtained. This value is slightly below the apparent pK_a value of 9.4 obtained using a simple kinetic model to interpret time-resolved optical spectroscopy experiments,[70] as well as the pK_a values between 8 and 12 calculated using other computational methods,[66,71] but it is consistent with the uncertainty of ± 1 pK_a unit typically obtained with computational estimates.[42,72,73] This unusually high pK_a value means that this residue is mostly protonated at neutral pH. This has been proposed to provide a mechanism through which the leaking of protons back through the D-channel is prevented.[71] Although $E286_I$ is a buried residue, deprotonation and reprotonation of $E286_I$ have been observed experimentally by time-resolved ATR-FTIR spectroscopy,[74] which indicates that despite its relatively high pK_a value, the residue is able to change protonation state during the catalytic cycle of C*c*O.

In the case of $Y288_I$, a pK_a value of 7.4 was obtained. Even though this value is slightly above the value of 6.6 obtained for the oxidized state of C*c*O using FTIR,[75] this is again consistent with the typical uncertainty of ± 1 pK_a unit. The pK_a value of $Y288_I$ is lower than that of a tyrosine residue in solution largely due to its covalent bond to $H284_I$, which as previously reported, allows it do donate a proton during catalysis at physiological pH values.[63,64,76,77] The effect of this covalent bond is taken into account by the pK_a value of the model compound, i.e. the pK_a of the isolated group when it is completely solvated, being lower than that of a regular tyrosine, as previously described.[43,78]

Lastly, $K362_I$ is often believed to be neutral at physiological pH, as supported by the very low (even negative) pK_a values obtained in some computational studies.[69,79] However, some kinetic data suggest that this site may be actually charged at neutral pH during the catalytic cycle,[80] in agreement with our present pK_a value of 7.6 and the one obtained in another computational study.[81] The discrepancy between these computational

studies, all ultimately relying on a CE model to estimate ionization free energies, may largely result from the methodological details of each approach (e.g. structural sampling, treatment of water molecules, etc).

It is also interesting to compare the pK_a values reported here with the results of a recent study using constant-pH MD simulations at pH 7,[28] in which these three residues were observed to be neutral. This is consistent with the present pK_a values of 7.9 for E286$_I$ and 7.4 for Y288$_I$ (which indicate mostly neutral states at pH 7), but not with the pK_a of 7.6 for K362$_I$ (which indicates a mostly charged state at pH 7). However, given the use of a single pH value of 7 in the constant-pH MD study, together with the above-mentioned uncertainty around 1 pH unit expected from these calculations, it is difficult to judge the significance of this discrepancy for K362$_I$.

Influence of the pH gradient on key residues

Regarding the influence of the pH gradient on the titration of E286$_I$, Y288$_I$ and K362$_I$, Figure 3C shows how the titration curves of these residues are affected by the pH values on both sides of the membrane. We can observe that, in all three cases, the major influence comes from the pH of the side they are assigned to. This is why the two-dimensional titration curves of E286$_I$ and K362$_I$, both assigned to the N-side of the membrane, bear some similarity, particularly at physiological pH values (figure 3D), whereas Y288$_I$ is more influenced by the pH on the P-side. Like other residues affected by the pH gradient (see figure S3 in the SI), E286$_I$, Y288$_I$ and K362$_I$ display a consistent trend: if the pH of the membrane side to which they are assigned is kept fixed and the pH on the opposite side is increased, they tend to become more protonated, which may seem counterintuitive. This general trend is due to the fact that a pH increase on one side leads, through local proton exchange equilibrium, to a lower repulsion on protons at the other side. For example, if pH$_P$ is increased while pH$_N$ is fixed at 7-8, the residues assigned to (in equilibrium with) side P would tend to become less protonated, therefore reducing the electrostatic repulsion

exerted on protons potentially binding to residues assigned to side N, which thus tend to increase their protonation. This effect is noticeable only when residues assigned to different membrane sides are sufficiently close to electrostatically affect each other, which explains why few residues display this behavior. In all cases, the region we are most interested in is the region below the diagonal line in figures 3C and 3D, particularly when the pH on the N-side increases and the pH on the P-side decreases, which is what would be observed as protons are pumped from the N- to the P-side.

In the case of $E286_I$, we can observe that in this region, at pH values below neutrality, e.g. $pH_N \approx 6$ and $pH_P \approx 5$, $E286_I$ is still protonated, but starts to deprotonate as soon as the pH_N increases. Since $E286_I$ tends to deprotonate as the pH gradient increases, it would gradually become thermodynamically less prone to transfer either chemical protons to the binuclear center or pumped protons to the P-side of the membrane. Therefore, the persistent building of a pH gradient could eventually lead to a decrease in both the pumping and the catalytic activity of C*c*O.

Regarding $Y288_I$, as the pH_N increases and the pH_P decreases, $Y288_I$ appears to be almost exclusively protonated, particularly in the region where pH_N is over 6.5 and pH_P drops below 6.5. In this region, $Y288_I$ will prefer to hold on to its proton, rather than donate it to the oxygen molecule in the binuclear center, thereby thermodynamically hindering the catalytic activity of C*c*O. Therefore, a gradual increase of the pH gradient would eventually impair the transfer of chemical protons from $Y288_I$ to the binuclear center, which could lead to a reduction in the catalytic activity of the oxidase.

As for $K362_I$, despite being located approximately 15 Å away from the binuclear center, we can observe that its titration is also dependent on the pH gradient. When focusing once again on the region below the diagonal line (Figure 3D), as the pH_N increases and the pH_P decreases, $K362_I$ tends to become deprotonated. When $K362_I$ becomes deprotonated it is unable to transfer chemical protons to $Y288_I$ via the K-channel, which as we have previously mentioned, could also hinder the catalytic activity of the oxidase.

If we take into account the two-dimensional titration curves of all three residues, we can observe that as the pH gradient increases, $E286_I$ and $K362_I$ tend to deprotonate, and $Y288_I$ tends to become protonated. The trend observed seems to suggest that in the presence of large pH gradients (>2 pH units), key residues in both proton conducting channels of C*c*O tend to become unable to perform proton exchanges, thereby affecting both the proton pumping and the catalytic activity of the oxidase. Even though the differences in pH across the membrane are usually not this large (usually in the order of 0.5–1.0 pH units),[1,18] these results seem to suggest that these key residues may be part of a regulatory mechanism in C*c*O. As in similar CE/MC studies of proton transfer,[23,24,79] these results capture only the thermodynamic aspect of the transfer, which, although a major component of the energy barrier, is not the only determinant for the kinetics.[82,83]

Correlation between protonation states

Due to their known roles in the catalytic and proton pumping activities of C*c*O, and as we can observe in Figure 3A, it is no surprise that $E286_I$, $Y288_I$ and $K362_I$ are relatively close to each other. The distances between the Oε1 atom of $E286_I$, the Oη atom of $Y288_I$ and the Nζ atom of $K362_I$ were measured and found to be below 20 Å, as shown in Figure 4A. As done before,[23,25,84,85] and in order to better evaluate the effective interactions of these residues with each other as well as with other residues, we calculated the correlation between the protonations of all site pairs at all pH gradient values. The calculated correlations are normalized values as used in Refs. 25,84,85 which range from -1 (completely anti-correlated) to $+1$ (completely correlated). A positive correlation value means that two sites tend to be (de)protonated at the same time, and are, as such, correlated, whereas a negative correlation value means that the titration of two sites is anti-correlated, i.e. that one site tends to protonate when the other one deprotonates. A correlation value of zero means that the two sites are not correlated.

We can observe in Figure 4 that the protonations of the three key sites $E286_I$, $Y288_I$ and

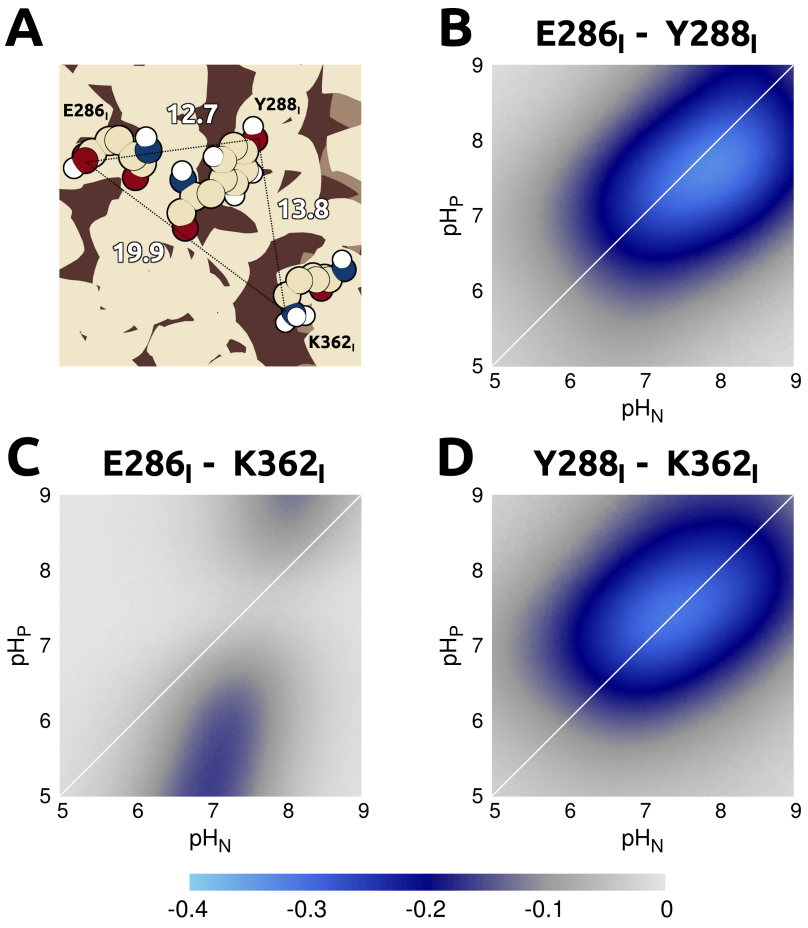

Figure 4: Distance (in Å) between $E286_I$, $Y288_I$ and $K362_I$ (A) and the correlation between the protonation states of all three sites (B-D). The minima are located at: -0.34 at (pH_N,pH_P) = (7.9,7.6) (B), -0.16 at (pH_N,pH_P) = (6.9,5.1) (C), and -0.32 at (pH_N,pH_P) = (7.4,7.4) (D).

$K362_I$ exhibit a small anti-correlation. Figures 4B and D show that the protonation of $Y288_I$ is negatively correlated with both $E286_I$ and $K362_I$ in the region where all three residues are titrating. These results indicate that when $Y288_I$ is protonated in this pH range, it is unlikely that either $E286_I$ or $K362_I$ are simultaneously protonated. In addition, despite the larger distance between $E286_I$ and $K362_I$, together with the fact that they belong to different proton conducing pathways, the protonations of these two residues appear to be negatively correlated, as we can observe in Figure 4C. This negative correlation occurs roughly along the same region where both would be titrating (i.e. where their yellow regions in Figure 3D approximately overlap), which is not surprising. It is interesting to note however, that in the area which coincides with the region where $Y288_I$ is titrating, the protonation of the $E286_I$ and $K362_I$ ceases to be negatively correlated, which suggests that the titration of $Y288_I$ may lead to the D- and K-channels operating independently. Taken together, these results suggest a possible role of $Y288_I$ in the regulation of proton transfer (Fig. 5). In the pH range where $Y288_I$ is not titrating, either $E286_I$ or $K362_I$ tend to be protonated, meaning that either the D- or the K-channel can transfer protons, whereas when $Y288_I$ is titrating, $E286_I$ and $K362_I$ lose their anti-correlation and become more likely to be simultaneously protonated, meaning that both channels could be working at the same time. It has been previously suggested that $E286_I$ could fulfill such a role,[47,65,66] either by itself or as part of a network of interacting residues, given that it is a key component of the D-channel, which transports both chemical protons to the binuclear center and pumped protons from the N- to the P-side of the membrane. However, despite $Y288_I$ being part of the K-channel, which only transports chemical protons, its relative proximity to $E286_I$ (and thus, the D-channel) and its known role in catalysis make it also a candidate for the regulation of proton flow. Although some experimental studies indicate that an increase in ΔpH negatively impacts the activity of C*c*O, in agreement with the regulatory mechanism here proposed, they were done with additional C*c*O subunits or additional respiratory complexes present, and no connection was established with particular C*c*O residues.[21,22]

Therefore, further studies, possibly involving the remaining intermediates of the reaction cycle, are required in order to test this hypothesis.

It should be noted that the correlations between these three residues may be affected by structural reorganization, which his here simply modeled through a moderately higher dielectric constant for the protein interior. As noted above, a recent constant-pH MD study, allowing for changes of both protonation and conformation in C*c*O[28] did not show (de)protonation events of these three residues, but $E286_I$ and $K362_I$ were found to display substantial flexibility, which other studies suggested to be coupled with (de)protonation (e.g. see references 47,69,86). Further studies with explicit structural flexibility are needed to elucidate these correlations.

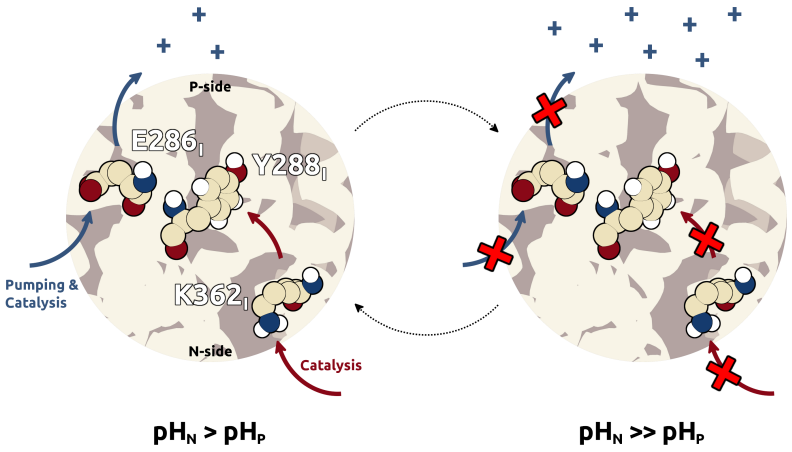

Figure 5: Schematic representation of the proposed regulatory mechanism in C*c*O. The figure on the left shows a close-up of $E286_I$, $Y288_I$ and $K362_I$, with blue and red arrows depicting the flow of protons in the D- and K-channels, respectively, with protons transferred from the N- to the P-side contributing to the formation of a pH gradient. As the gradient becomes larger (right), and the titration of the three residues moves further away from the midpoint (fig. 3C and D), they become unable to exchange protons and, as such, the catalytic and proton pumping activities of C*c*O become impaired. Once this proton transfer is blocked, the lower pH gradient can be reestablished by other proton fluxes (ATP synthase, etc), then restoring the proton transfer ability of these three residues.

Conclusions

In this work, we studied the effects of the pH gradient on the protonation states of residues in cytochrome *c* oxidase. By including ΔpH in our CE/MC method, we found three different types of titration behavior, as it was also observed in the case of bacteriorhodopsin:[23] residues that did not titrate, residues whose titration was only affected by the pH of the side they were assigned to, and residues whose titration was affected by the pH gradient. Among the residues whose titration depended on the pH gradient, three were found to be particularly relevant: $E286_I$, $Y288_I$ and $K362_I$. All three of these residues were previously identified as key residues involved in proton transfer. We determined the pK_a values for these three sites in the absence of a pH gradient and found that there was agreement with previous studies in the case of $E286_I$ and $Y288_I$ (within 0.8–1.5 pK units), while our result for $K362_I$ supports previous studies proposing a pK_a around neutrality, rather than those proposing a very low pK_a.

Regarding the influence of the pH gradient on the titration of these residues, we found that, as the gradient increases (i.e. pH_N increases and pH_P decreases), $E286_I$, $Y288_I$ and $K362_I$ become less prone to exchange protons. We have also found that, in this gradient region, the protonation of these residues shows some anti-correlation, which means that usually when one of them becomes protonated, the others tend to become deprotonated. Given their role in the proton transfer pathways of C*c*O, if any of these residues is unable to exchange a proton, the catalytic and proton pumping activities of C*c*O become impaired. These results suggest that these residues may be part of a regulatory mechanism to control the proton flow if the gradient becomes too large (Fig. 5).

The present study shows that, as previously found by others,[23] the inclusion of a transmembrane pH gradient in CE/MC calculations enables the detection of residues whose titration is influenced by the pH gradient. In the particular case of C*c*O, this allowed us to find that well known key sites involved in the proton transfer mechanism of this enzyme are sensitive to this gradient and possibly involved on regulation mechanisms.

Therefore, this approach seems to be a valuable tool for the study of proton transfer in systems experiencing a pH gradient.

Acknowledgement

This study was supported by Project LISBOA-01-0145-FEDER-007660 (Microbiologia Molecular, Estrutural e Celular) funded by FEDER funds through COMPETE2020 - Programa Operacional Competitividade e Internacionalização (POCI) and by national funds through FCT - Fundação para a Ciência e a Tecnologia, Portugal. Funding was also provided by FCT through the following grants: SFRH/BD/ 65709/2009, SFRH/BPD/76621/2011, PTDC/QEQ-COM/1623/2012, Pest-OE/ EQB/LA0004/2011. We thank Dr. Manuela Pereira for the helpful discussions.

Supporting Information Available

Atomic partial charges of the bacteriorhodopsin retinal group; two-dimensional titration curves of bacteriorhodopsin residues; two-dimensional titration curves of all C*c*O residues; pK_a values of all titratable sites of C*c*O. This material is available free of charge via the Internet at `http://pubs.acs.org/`.

References

(1) Nicholls, D. G.; Ferguson, S. J. *Bioenergetics, Third Edition*, 3rd ed.; Academic Press, 2002.

(2) Pereira, M. M.; Santana, M.; Teixeira, M. A Novel Scenario for the Evolution of Haem–Copper Oxygen Reductases. *Biochim. Biophys. Acta, Bioenerg.* **2001**, *1505*, 185–208.

(3) Brzezinski, P.; Gennis, R. B. Cytochrome *c* Oxidase: Exciting Progress and Remaining Mysteries. *J. Bioenerg. Biomembr.* **2008**, *40*, 521–531.

(4) DeLano, W. The PyMOL Molecular Graphics System. 2002.

(5) GIMP 2.8.10, www.gimp.org. 1997-2016.

(6) Konstantinov, A. A.; Siletsky, S.; Mitchell, D.; Kaulen, A.; Gennis, R. B. The Roles of the Two Proton Input Channels in Cytochrome *c* Oxidase from *Rhodobacter sphaeroides* Probed by the Effects of Site-Directed Mutations on Time-Resolved Electrogenic Intraprotein Proton Transfer. *Proc. Natl. Acad. Sci. U. S. A.* **1997**, *94*, 9085–9090.

(7) Siletsky, S. A. Steps of the Coupled Charge Translocation in the Catalytic Cycle of Cytochrome *c* Oxidase. *Front. Biosci., Landmark Ed.* **2012**, *18*, 36–57.

(8) Brändén, M.; Tomson, F.; Gennis, R. B.; Brzezinski, P. The Entry Point of the K-Proton-Transfer Pathway in Cytochrome *c* Oxidase. *Biochemistry* **2002**, *41*, 10794–10798.

(9) Tomson, F. L.; Morgan, J. E.; Gu, G.; Barquera, B.; Vygodina, T.; Gennis, R. B. Substitutions for Glutamate 101 in Subunit II of Cytochrome *c* Oxidase from *Rhodobacter sphaeroides* Result in Blocking the Proton-Conducting K-Channel. *Biochemistry* **2003**, *42*, 1711–1717.

(10) Brzezinski, P.; Johansson, A.-L. Variable Proton-Pumping Stoichiometry in Structural Variants of Cytochrome *c* Oxidase. *Biochim. Biophys. Acta, Bioenerg.* **2010**, *1797*, 710–723.

(11) Gennis, R. B. Multiple Proton-Conducting Pathways in Cytochrome Oxidase and a Proposed Role for the Active-Site Tyrosine. *Biochim. Biophys. Acta, Bioenerg.* **1998**, *1365*, 241–248.

(12) Tsukihara, T.; Shimokata, K.; Katayama, Y.; Shimada, H.; Muramoto, K.; Aoyama, H.; Mochizuki, M.; Shinzawa-Itoh, K.; Yamashita, E.; Yao, M.; Ishimura, Y.; Yoshikawa, S.

The Low-Spin Heme of Cytochrome *c* Oxidase as the Driving Element of the Proton-Pumping Process. *Proc. Natl. Acad. Sci. U. S. A.* **2003**, *100*, 15304–15309.

(13) Shimokata, K.; Katayama, Y.; Murayama, H.; Suematsu, M.; Tsukihara, T.; Muramoto, K.; Aoyama, H.; Yoshikawa, S.; Shimada, H. The Proton Pumping Pathway of Bovine Heart Cytochrome *c* Oxidase. *Proc. Natl. Acad. Sci. U. S. A.* **2007**, *104*, 4200–4205.

(14) Jünemann, S.; Meunier, B.; Gennis, R. B.; Rich, P. R. Effects of Mutation of the Conserved Lysine-362 in Cytochrome *c* Oxidase from *Rhodobacter sphaeroides*. *Biochemistry* **1997**, *36*, 14456–14464.

(15) Rich, P.; Jünemann, S.; Meunier, B. Protonmotive Mechanism of Heme-Copper Oxidases. *J. Bioenerg. Biomembr.* **1998**, *30*, 131–138.

(16) Rich, P. R.; Maréchal, A. Functions of the Hydrophilic Channels in Protonmotive Cytochrome *c* Oxidase. *J. R. Soc., Interface* **2013**, *10*, 20130183.

(17) Gunner, M.; Amin, M.; Zhu, X.; Lu, J. Molecular Mechanisms for Generating Transmembrane Proton Gradients. *Biochim. Biophys. Acta, Bioenerg.* **2013**, *1827*, 892–913.

(18) Mitchell, P.; Moyle, J. Estimation of Membrane Potential and pH Difference Across the Cristae Membrane of Rat Liver Mitochondria. *Eur. J. Biochem.* **1969**, *7*, 471–484.

(19) Moroney, P. M.; Scholes, T. A.; Hinkle, P. C. Effect of Membrane Potential and pH Gradient on Electron Transfer in Cytochrome Oxidase. *Biochemistry* **1984**, *23*, 4991–4997.

(20) Nomura, T.; Yanagisawa, S.; Shinzawa-Itoh, K.; Yoshikawa, S.; Ogura, T. Effects of Proton Motive Force on the Structure and Dynamics of Bovine Cytochrome *c* Oxidase in Phospholipid Vesicles. *Biochemistry* **2014**, *53*, 6382–6391.

(21) Capitanio, N.; Capitanio, G.; Demarinis, D.; De Nitto, E.; Massari, S.; Papa, S. Factors Affecting the H^+/e^--Stoichiometry in Mitochondrial Cytochrome *c* Oxidase: Influence of the Rate of Electron Flow and Transmembrane ΔpH. *Biochemistry* **1996**, *35*, 10800–10806.

(22) Quarato, G.; Piccoli, C.; Scrima, R.; Capitanio, N. Variation of Flux Control Coefficient of Cytochrome *c* Oxidase and of the Other Respiratory Chain Complexes at Different Values of Protonmotive Force Occurs by a Threshold Mechanism. *Biochim. Biophys. Acta, Bioenerg.* **2011**, *1807*, 1114–1124.

(23) Calimet, N.; Ullmann, G. M. The Influence of a Transmembrane pH Gradient on Protonation Probabilities of Bacteriorhodopsin: The Structural Basis of the Back-Pressure Effect. *J. Mol. Biol.* **2004**, *339*, 571–589.

(24) Bombarda, E.; Becker, T.; Ullmann, G. M. Influence of the Membrane Potential on the Protonation of Bacteriorhodopsin: Insights from Electrostatic Calculations into the Regulation of Proton Pumping. *J. Am. Chem. Soc.* **2006**, *128*, 12129–12139.

(25) Baptista, A. M.; Martel, P. J.; Soares, C. M. Simulation of Electron-Proton Coupling With a Monte Carlo Method: Application to Cytochrome c_3 Using Continuum Electrostatics. *Biophys. J.* **1999**, *76*, 2978–2998.

(26) Baptista, A. M.; Soares, C. M. Some Theoretical and Computational Aspects of the Inclusion of Proton Isomerism in the Protonation Equilibrium of Proteins. *J. Phys. Chem. B* **2001**, *105*, 293–309.

(27) Qin, L.; Hiser, C.; Mulichak, A.; Garavito, R. M.; Ferguson-Miller, S. Identification of Conserved Lipid/Detergent-Binding Sites in a High-Resolution Structure of the Membrane Protein Cytochrome *c* Oxidase. *Proc. Natl. Acad. Sci. U. S. A.* **2006**, *103*, 16117–16122.

(28) Oliveira, A. S. F.; Campos, S. R.; Baptista, A. M.; Soares, C. M. Coupling Between Protonation and Conformation in Cytochrome *c* Oxidase: Insights from Constant-pH MD Simulations. *Biochim. Biophys. Acta, Bioenerg.* **2016**, *1857*, 759–771.

(29) Berendsen, H. J. C.; van der Spoel, D.; van Drunen, R. GROMACS: A Message-Passing Parallel Molecular Dynamics Implementation. *Comput. Phys. Commun.* **1995**, *91*, 43–56.

(30) Hess, B.; Kutzner, C.; van der Spoel, D.; Lindahl, E. GROMACS 4: Algorithms for Highly Efficient, Load-Balanced, and Scalable Molecular Simulation. *J. Chem. Theory Comput.* **2008**, *4*, 435–447.

(31) Hermans, J.; Berendsen, H. J. C.; Van Gunsteren, W. F.; Postma, J. P. M. A Consistent Empirical Potential for Water–Protein Interactions. *Biopolymers* **1984**, *23*, 1513–1518.

(32) Press, W.; Teukolsky, S.; Vetterling, W.; Flannery, B. *Numerical Recipes in C, the Art of Scientific Computing*, cambridge university press ed.; 1992.

(33) Eisenhaber, F.; Argos, P. Improved Strategy in Analytic Surface Calculation for Molecular Systems: Handling of Singularities and Computational Efficiency. *J. Comput. Chem.* **1993**, *14*, 1272–1280.

(34) Eisenhaber, F.; Lijnzaad, P.; Argos, P.; Sander, C.; Scharf, M. The Double Cubic Lattice Method: Efficient Approaches to Numerical Integration of Surface Area and Volume and to Dot Surface Contouring of Molecular Assemblies. *J. Comput. Chem.* **1995**, *16*, 273–284.

(35) Schmid, N.; Eichenberger, A. P.; Choutko, A.; Riniker, S.; Winger, M.; Mark, A. E.; van Gunsteren, W. F. Definition and Testing of the GROMOS Force-Field Versions 54A7 and 54B7. *Eur. Biophys. J.* **2011**, *40*, 843–856.

(36) Berendsen, H. In *Molecular Dynamics and Protein Structure: Proceedings of a Workshop*

Held 13-18 May 1984 at the University of North Carolina; Hermans, J., Ed.; University of North Carolina, Distributed by Polycrystal Book Service: Western Springs Ill., 1985.

(37) Tironi, I. G.; Sperb, R.; Smith, P. E.; van Gunsteren, W. F. A Generalized Reaction Field Method for Molecular Dynamics Simulations. *J. Chem. Phys.* **1995**, *102*, 5451–5459.

(38) Hess, B.; Bekker, H.; Berendsen, H. J.; Fraaije, J. G. LINCS: A Linear Constraint Solver for Molecular Simulations. *J. Comput. Chem.* **1997**, *18*, 1463–1472.

(39) Bussi, G.; Donadio, D.; Parrinello, M. Canonical Sampling Through Velocity Rescaling. *J. Chem. Phys.* **2007**, *126*, 014101.

(40) Berendsen, H. J. C.; Postma, J. P. M.; van Gunsteren, W. F.; DiNola, A.; Haak, J. R. Molecular Dynamics with Coupling to an External Bath. *J. Chem. Phys.* **1984**, *81*, 3684–3690.

(41) Bashford, D.; Gerwert, K. Electrostatic Calculations of the pK_a Values of Ionizable Groups in Bacteriorhodopsin. *J. Mol. Biol.* **1992**, *224*, 473–486.

(42) Teixeira, V. H.; Cunha, C. A.; Machuqueiro, M.; Oliveira, A. S. F.; Victor, B. L.; Soares, C. M.; Baptista, A. M. On the Use of Different Dielectric Constants for Computing Individual and Pairwise Terms in Poisson-Boltzmann Studies of Protein Ionization Equilibrium. *J. Phys. Chem. B* **2005**, *109*, 14691–14706.

(43) Oliveira, A. S. F.; Damas, J. a. M.; Baptista, A. M.; Soares, C. M. Exploring O_2 Diffusion in A-Type Cytochrome *c* Oxidases: Molecular Dynamics Simulations Uncover Two Alternative Channels Towards the Binuclear Site. *PLoS Comput. Biol.* **2014**, *10*, e1004010.

(44) Eberini, I.; Baptista, A. M.; Gianazza, E.; Fraternali, F.; Beringhelli, T. Reorganization in Apo- and Holo-β-Lactoglobulin upon Protonation of Glu89: Molecular Dynamics and pK_a Calculations. *Proteins: Struct., Funct., Bioinf.* **2004**, *54*, 744–758.

(45) Schutz, C. N.; Warshel, A. What Are the Dielectric "Constants" of Proteins and How to Validate Electrostatic Models? *Proteins: Struct., Funct., Bioinf.* **2001**, *44*, 400–417.

(46) Teixeira, V. H.; Vila-Viçosa, D.; Baptista, A. M.; Machuqueiro, M. Protonation of DMPC in a Bilayer Environment Using a Linear Response Approximation. *J. Chem. Theory Comput.* **2014**, *10*, 2176–2184.

(47) Kaila, V. R.; Verkhovsky, M.; Hummer, G.; Wikström, M. Prevention of Leak in the Proton Pump of Cytochrome *c* Oxidase. *Biochim. Biophys. Acta, Bioenerg.* **2008**, *1777*, 890–892.

(48) Metropolis, N.; Rosenbluth, A. W.; Rosenbluth, M. N.; Teller, A. H.; Teller, E. Equation of State Calculations by Fast Computing Machines. *J. Chem. Phys.* **1953**, *21*, 1087–1092.

(49) Lanyi, J. K. Bacteriorhodopsin. *Annu. Rev. Physiol.* **2004**, *66*, 665–688.

(50) Luecke, H.; Schobert, B.; Richter, H. T.; Cartailler, J. P.; Lanyi, J. K. Structure of Bacteriorhodopsin at 1.55 Å Resolution. *J. Mol. Biol.* **1999**, *291*, 899–911.

(51) Sali, A.; Blundell, T. L. Comparative Protein Modelling by Satisfaction of Spatial Restraints. *J. Mol. Biol.* **1993**, *234*, 779–815.

(52) Fiser, A.; Do, R. K.; Sali, A. Modeling of Loops in Protein Structures. *Protein Sci.* **2000**, *9*, 1753–1773.

(53) Martí-Renom, M. A.; Stuart, A. C.; Fiser, A.; Sánchez, R.; Melo, F.; Sali, A. Comparative Protein Structure Modeling of Genes and Genomes. *Annu. Rev. Biophys. Biomol. Struct.* **2000**, *29*, 291–325.

(54) Eswar, N.; Webb, B.; Marti-Renom, M. A.; Madhusudhan, M. S.; Eramian, D.; Shen, M.-Y.; Pieper, U.; Sali, A. Comparative Protein Structure Modeling Using Modeller. *Curr. Protoc. Bioinform.* **2006**, *Chapter 5*, Unit 5.6.

(55) Belrhali, H.; Nollert, P.; Royant, A.; Menzel, C.; Rosenbusch, J. P.; Landau, E. M.; Pebay-Peyroula, E. Protein, Lipid and Water Organization in Bacteriorhodopsin Crystals: A Molecular View of the Purple Membrane at 1.9 Å Resolution. *Structure* **1999**, *7*, 909–917.

(56) Frisch, M. J.; Trucks, G. W.; Schlegel, H. B.; Scuseria, G. E.; Robb, M. A.; Cheeseman, J. R.; Scalmani, G.; Barone, V.; Mennucci, B.; Petersson, G. A.; Nakatsuji, H.; Caricato, M.; Li, X.; Hratchian, H. P.; Izmaylov, A. F.; Bloino, J.; Zheng, G.; Sonnenberg, J. L.; Hada, M.; Ehara, M.; Toyota, K.; Fukuda, R.; Hasegawa, J.; Ishida, M.; Nakajima, T.; Honda, Y.; Kitao, O.; Nakai, H.; Vreven, T.; Montgomery, J. A., Jr.; Peralta, J. E.; Ogliaro, F.; Bearpark, M.; Heyd, J. J.; Brothers, E.; Kudin, K. N.; Staroverov, V. N.; Kobayashi, R.; Normand, J.; Raghavachari, K.; Rendell, A.; Burant, J. C.; Iyengar, S. S.; Tomasi, J.; Cossi, M.; Rega, N.; Millam, N. J.; Klene, M.; Knox, J. E.; Cross, J. B.; Bakken, V.; Adamo, C.; Jaramillo, J.; Gomperts, R.; Stratmann, R. E.; Yazyev, O.; Austin, A. J.; Cammi, R.; Pomelli, C.; Ochterski, J. W.; Martin, R. L.; Morokuma, K.; Zakrzewski, V. G.; Voth, G. A.; Salvador, P.; Dannenberg, J. J.; Dapprich, S.; Daniels, A. D.; Farkas, O.; Foresman, J. B.; Ortiz, J. V.; Cioslowski, J.; Fox, D. J. Gaussian 09, Revision A.1. 2009.

(57) Bayly, C. I.; Cieplak, P.; Cornell, W.; Kollman, P. A. A Well-Behaved Electrostatic Potential Based Method Using Charge Restraints for Deriving Atomic Charges: The RESP Model. *J. Phys. Chem.* **1993**, *97*, 10269–10280.

(58) Senn, H. M.; Thiel, W. QM/MM Methods for Biomolecular Systems. *Angew. Chem., Int. Ed.* **2009**, *48*, 1198–1229.

(59) Kannt, A.; Lancaster, C. R. D.; Michel, H. The Coupling of Electron Transfer and Proton Translocation: Electrostatic Calculations on *Paracoccus denitrificans* Cytochrome *c* Oxidase. *Biophys. J.* **1998**, *74*, 708–721.

(60) Beroza, P.; Fredkin, D. R.; Okamura, M. Y.; Feher, G. Electrostatic Calculations of Amino Acid Titration and Electron Transfer, $Q_A^- Q_B \rightarrow Q_A Q_B^-$, in the Reaction Center. *Biophys. J.* **1995**, *68*, 2233–2250.

(61) Williams, T.; Kelley, C. Gnuplot. 2004.

(62) Lee, H.-m.; Das, T. K.; Rousseau, D. L.; Mills, D.; Ferguson-Miller, S.; Gennis, R. B. Mutations in the Putative H-Channel in the Cytochrome *c* Oxidase from *Rhodobacter sphaeroides* Show that this Channel Is Not Important for Proton Conduction but Reveal Modulation of the Properties of Heme *a*. *Biochemistry* **2000**, *39*, 2989–2996.

(63) Ostermeier, C.; Harrenga, A.; Ermler, U.; Michel, H. Structure at 2.7 Å Resolution of the *Paracoccus denitrificans* Two-Subunit Cytochrome *c* Oxidase Complexed with an Antibody FV Fragment. *Proc. Natl. Acad. Sci. U. S. A.* **1997**, *94*, 10547–10553.

(64) Yoshikawa, S.; Shinzawa-Itoh, K.; Nakashima, R.; Yaono, R.; Yamashita, E.; Inoue, N.; Yao, M.; Fei, M. J.; Libeu, C. P.; Mizushima, T.; Yamaguchi, H.; Tomizaki, T.; Tsukihara, T. Redox-Coupled Crystal Structural Changes in Bovine Heart Cytochrome *c* Oxidase. *Science* **1998**, *280*, 1723–1729.

(65) Kaila, V. R.; Verkhovsky, M. I.; Hummer, G.; Wikström, M. Glutamic Acid 242 Is a Valve in the Proton Pump of Cytochrome *c* Oxidase. *Proc. Natl. Acad. Sci. U. S. A.* **2008**, *105*, 6255–6259.

(66) Woelke, A. L.; Galstyan, G.; Galstyan, A.; Meyer, T.; Heberle, J.; Knapp, E.-W. Exploring the Possible Role of Glu286 in C*c*O by Electrostatic Energy Computations Combined with Molecular Dynamics. *J. Phys. Chem. B* **2013**, *117*, 12432–12441.

(67) Iwata, S.; Ostermeier, C.; Ludwig, B.; Michel, H. Structure at 2.8 Å Resolution of Cytochrome *c* Oxidase from *Paracoccus denitrificans*. *Nature* **1995**, *376*, 660–668.

(68) Hofacker, I.; Schulten, K. Oxygen and Proton Pathways in Cytochrome *c* Oxidase. *Proteins: Struct., Funct., Genet.* **1998**, *30*, 100–107.

(69) Woelke, A. L.; Galstyan, G.; Knapp, E.-W. Lysine 362 in Cytochrome *c* Oxidase Regulates Opening of the K-Channel Via Changes in pK_a and Conformation. *Biochim. Biophys. Acta, Bioenerg.* **2014**, *1837*, 1998–2003.

(70) Namslauer, A.; Aagaard, A.; Katsonouri, A.; Brzezinski, P. Intramolecular Proton-Transfer Reactions in a Membrane-Bound Proton Pump: The Effect of pH on the Peroxy to Ferryl Transition in Cytochrome *c* Oxidase. *Biochemistry* **2003**, *42*, 1488–1498.

(71) Fadda, E.; Yu, C.-H.; Pomès, R. Electrostatic Control of Proton Pumping in Cytochrome *c* Oxidase. *Biochim. Biophys. Acta, Bioenerg.* **2008**, *1777*, 277–284.

(72) Davies, M. N.; Toseland, C. P.; Moss, D. S.; Flower, D. R. Benchmarking pK_a Prediction. *BMC Biochem.* **2006**, *7*, 1–12.

(73) Stanton, C. L.; Houk, K. N. Benchmarking pK_a Prediction Methods for Residues in Proteins. *J. Chem. Theory Comput.* **2008**, *4*, 951–966.

(74) Gorbikova, E. A.; Belevich, N. P.; Wikström, M.; Verkhovsky, M. I. Time-Resolved ATR-FTIR Spectroscopy of the Oxygen Reaction in the D124N Mutant of Cytochrome *c* Oxidase from *Paracoccus denitrificans*. *Biochemistry* **2007**, *46*, 13141–13148.

(75) Gorbikova, E. A.; Wikström, M.; Verkhovsky, M. I. The Protonation State of the Cross-Linked Tyrosine During the Catalytic Cycle of Cytochrome *c* Oxidase. *J. Biol. Chem.* **2008**, *283*, 34907–34912.

(76) McCauley, K. M.; Vrtis, J. M.; Dupont, J.; van der Donk, W. A. Insights into the Functional Role of the Tyrosine-Histidine Linkage in Cytochrome *c* Oxidase. *J. Am. Chem. Soc.* **2000**, *122*, 2403–2404.

(77) Svensson-Ek, M.; Abramson, J.; Larsson, G.; Törnroth, S.; Brzezinski, P.; Iwata, S. The X-Ray Crystal Structures of Wild-Type and EQ (I-286) Mutant Cytochrome *c* Oxidases from *Rhodobacter sphaeroides*. *J. Mol. Biol.* **2002**, *321*, 329–339.

(78) Soares, C. M.; Baptista, A. M.; Pereira, M. M.; Teixeira, M. Investigation of Protonatable Residues in *Rhodothermus marinus* caa_3 Haem-Copper Oxygen Reductase: Comparison with *Paracoccus denitrificans* aa_3 Haem-Copper Oxygen Reductase. *JBIC, J. Biol. Inorg. Chem.* **2004**, *9*, 124–134.

(79) Song, Y.; Michonova-Alexova, E.; Gunner, M. Calculated Proton Uptake on Anaerobic Reduction of Cytochrome *c* Oxidase: Is the Reaction Electroneutral? *Biochemistry* **2006**, *45*, 7959–7975.

(80) Brändén, M.; Sigurdson, H.; Namslauer, A.; Gennis, R. B.; Ädelroth, P.; Brzezinski, P. On the Role of the K-Proton Transfer Pathway in Cytochrome *c* Oxidase. *Proc. Natl. Acad. Sci. U. S. A.* **2001**, *98*, 5013–5018.

(81) Tuukkanen, A.; Verkhovsky, M. I.; Laakkonen, L.; Wikström, M. The K-pathway Revisited: A Computational Study on Cytochrome *c* Oxidase. *Biochim. Biophys. Acta, Bioenerg.* **2006**, *1757*, 1117–1121.

(82) Churg, A. K.; Weiss, R. M.; Warshel, A.; Takano, T. On the Action of Cytochrome *c*: Correlating Geometry Changes upon Oxidation with Activation Energies of Electron Transfer. *J. Phys. Chem.* **1983**, *87*, 1683–1694.

(83) Marcus, R. A.; Sutin, N. Electron Transfers in Chemistry and Biology. *Biochim. Biophys. Acta, Rev. Bioenerg.* **1985**, *811*, 265–322.

(84) Teixeira, V. H.; Soares, C. M.; Baptista, A. M. Studies of the Reduction and Protonation Behavior of Tetraheme Cytochromes Using Atomic Detail. *JBIC, J. Biol. Inorg. Chem.* **2002**, *7*, 200–216.

(85) Teixeira, V. H.; Soares, C. M.; Baptista, A. M. Proton Pathways in a [NiFe]-Hydrogenase: A Theoretical Study. *Proteins: Struct., Funct., Bioinf.* **2008**, *70*, 1010–1022.

(86) Yamashita, T.; Voth, G. A. Insights Into the Mechanism of Proton Transport in Cytochrome *c* Oxidase. *J. Am. Chem. Soc.* **2012**, *134*, 1147–1152.

Graphical TOC Entry